Organic Aerosols in Anoxic and Oxic Atmospheres of Earth-like Exoplanets: VUV-MIR Spectroscopy of CHON Tholins

Lisseth Gavilan, Nathalie Carrasco, Søren Vrønning Hoffmann, Nykola C. Jones, Nigel Mason

▶ **To cite this version:**

Lisseth Gavilan, Nathalie Carrasco, Søren Vrønning Hoffmann, Nykola C. Jones, Nigel Mason. Organic Aerosols in Anoxic and Oxic Atmospheres of Earth-like Exoplanets: VUV-MIR Spectroscopy of CHON Tholins. The Astrophysical Journal Letters, 2018, 861 (2), pp.art. 110. ⟨10.3847/1538-4357/aac8df⟩. ⟨insu-02087590⟩

HAL Id: insu-02087590

https://insu.hal.science/insu-02087590v1

Submitted on 2 Apr 2019

HAL is a multi-disciplinary open access archive for the deposit and dissemination of scientific research documents, whether they are published or not. The documents may come from teaching and research institutions in France or abroad, or from public or private research centers.

L'archive ouverte pluridisciplinaire **HAL**, est destinée au dépôt et à la diffusion de documents scientifiques de niveau recherche, publiés ou non, émanant des établissements d'enseignement et de recherche français ou étrangers, des laboratoires publics ou privés.

HAL Authorization

Draft version April 20, 2018
Typeset using LaTeX **twocolumn** style in AASTeX61

ORGANIC AEROSOLS IN ANOXIC AND OXIC ATMOSPHERES OF EARTH-LIKE EXOPLANETS: VUV-MIR SPECTROSCOPY OF CHON THOLINS

Lisseth Gavilan,[1] Nathalie Carrasco,[1] Søren Vrønning Hoffmann,[2] Nykola C. Jones,[2] and Nigel J. Mason[3]

[1] *LATMOS, Université Versailles St Quentin, UPMC Université Paris 06, CNRS, 11 blvd d'Alembert, 78280 Guyancourt, France*
[2] *ISA, Department of Physics and Astronomy, Aarhus University, Ny Munkegade 120, DK-8000 Aarhus C, Denmark*
[3] *Department of Physical Sciences, The Open University, Milton Keynes MK7 6AA, UK*

ABSTRACT

Organic hazes can drastically impact the characterization and detection of exoplanet atmospheres. We explore the effects of the transition from an anoxic to oxic atmosphere on the molecular structure of organic aerosols, by producing aerosols in N_2:CO_2:CH_4-rich plasmas with increasing CO_2/CH_4 gas ratios. We performed a spectroscopic study on the resulting aerosol analogs, CHON-rich tholins, from the vacuum-ultraviolet (VUV) to the mid-infrared (MIR), i.e. the 0.13 - 10 μm range. VUV spectroscopy revealed the presence of π - π^* and n - π^* transitions in the 200 - 500 nm range in all samples. These are attributed to electronic transitions in amine groups. As the CO_2/CH_4 ratio increases, new bands emerge that can be attributed to electronic transitions in hydroxyl and carboxyl functional groups. MIR spectroscopy showed that the molecular structure of oxidized aerosols is dominated by the CO_2/CH_4 ratio. Band deconvolution revealed the oxygenation of the organic matrix via the formation of oxygenated functional groups including amide, hydroxyl, and carbonyl groups. For the most oxidized aerosols absorption is greatest in the 0.13 - 0.3 μm and 6 - 10 μm regions. Some of the oxidized samples were further irradiated with VUV photons, resulting in the formation of π - π^* bands in the 200 - 250 nm region and a decrease in the band intensities below 200 nm, attributed to amine and nitrile losses. We discuss how oxidized aerosols could provide a detectable [bio]-signature in exoplanet atmospheres.

Keywords: Planets and satellites: atmospheres, fundamental parameters - Methods: laboratory: solid state - Techniques: spectroscopic

Corresponding author: Lisseth Gavilan
lisseth.gavilan@latmos.ipsl.fr

1. INTRODUCTION

Photochemical aerosols are present across the atmospheres of several bodies in the Solar system. These can be observed as hazes from the stratosphere to the ionosphere. As such, and depending on their optical properties, morphology and size distribution, they could heavily impact the radiative transfer of solar radiation and planetary surface temperature. One of the most notable examples of an atmosphere dominated by photochemical aerosols is Titan. Its quasi-reducing atmospheric chemistry is the result of photon and energetic particles (protons, cosmic rays) impact on N_2 and CH_4, an efficient gas mixture for the generation of organic photochemical aerosols (Wilson & Atreya 2004; Lavvas et al. 2013).

On Earth organic aerosols are presently one of the largest drivers of radiative forcing, affecting the Earth's thermal balance and providing a mechanism for climate change (Jacobson et al. 2000). In the Archean Earth (∼4 - 2.5 Gyr ago) the presence of photochemical aerosols could have influenced early planetary habitability via radiative shielding and surface cooling (Pavlov et al. 2001). Unlike Titan's anoxic atmosphere, CO_2 is expected to have been present in the atmosphere of Earth from its early stages following the emergence of life (Kasting 1993; Feulner 2012; von Paris et al. 2008). Atmospheric oxidation therefore probably impacted the formation and optical properties of early organic hazes (Haqq-Misra et al. 2008; Wolf & Toon 2010).

Aerosols are likely to be ubiquitous in the atmospheres of extrasolar planets (Marley et al. 2013) and their composition can be as widely varying as that of the exoplanetary atmospheres that they are formed in (Lavvas & Koskinen 2017). Methane was detected in the atmosphere of exoplanet HD 189733b (Swain et al. 2008) with CO, CO_2 and H_2O (Swain et al. 2009a). Swain et al. (2009b) detected H_2O, CH_4, and CO_2 in the near-infrared spectrum of exoplanet HD 209458b. CO_2 photodissociation is relevant to the radiative transfer in exoplanet atmospheres (Venot et al. 2017). Its presence could also affect the photochemical production of organic hazes in Earth-like exoplanets as shown by models, (Arney et al. 2017), and experiments (Trainer et al. 2006; Fleury et al. 2017; Gavilan et al. 2017).

While the optical properties of organic aerosols are needed to refine models of the Archean Earth and exoplanet atmospheres, their molecular properties are necessary to understand the spectral variations as a function of the degree of oxidation. The aim of this work is to experimentally simulate the composition of increasingly oxidizing atmospheres to understand the impact of CO_2 in the optical properties of the generated organic aerosols covering a wide spectral range, from the vacuum-ultraviolet to the mid-infrared. This study is a continuation of our first study on the UV-visible complex refractive indices of oxidized organic aerosols (Gavilan et al. 2017) but here we focus our study on the molecular, electronic and absorption properties of these aerosols.

2. EXPERIMENTS

Tholins were produced using the PAMPRE[1] experimental facility, a low-pressure (0.95 mbar) radiofrequency (RF) plasma reactor (Szopa et al. 2006). This apparatus allows the simulation of the complex organic chemistry initiated by energetic particles in planetary ionospheres. The 13.56 MHz RF source, set to 30 W, generates a capacitively coupled plasma fed by a gas mixture at 0.95 mbar. **The aerosol analogs presented in this study were prepared in a cold plasma where neutrals have a temperature of ∼340 K. However, the most observed exoplanets to date are hot giants (∼800 - 3000 K) and are particularly conducive to atmospheric observations (Madhusudhan et al. 2016). Future laboratory simulations under different temperatures and pressures should explore how these parameters could further impact the formation, composition and optical properties of aerosols. This paper is a first step in the investigation on the molecular properties of oxidized organic aerosols.**

Initially a gas mixture was chosen to simulate the reducing composition of Titan's atmosphere, i.e., N_2:CH_4 with a 95:5 ratio (e.g. Sciamma-O'Brien et al. 2012; Mahjoub et al. 2012). We then simulated increasingly oxidizing atmospheres by adding CO_2 to the N_2-CH_4 gas mixture. The resulting tholins, solids rich in C, H, O, and N (CHON-rich), are produced on substrates placed on the bottom electrode of the capacitor producing the plasma. One set of samples was prepared with a gas mixture keeping the N_2 partial pressure at 90%, while a second set of samples was prepared keeping the N_2 partial pressure at 95%. For both series, gas mixtures with CO_2:CH_4 ratios equal to **0, 1, 1.5 and 4 were used**. We can translate the CO_2:CH_4 ratios into C/O ratios, used to characterize exoplanet atmospheres in terms of their carbon content (e.g. Venot et al. 2015),

$$\frac{C}{O} = \frac{1 \times N_{CO_2} + 1 \times N_{CH_4}}{2 \times N_{CO_2}} = 0.5 + \frac{0.5}{CO_2 : CH_4} \quad (1)$$

[1] PAMPRE: Production d'Aérosols en Microgravité par Plasmas REactifs

Using this conversion we find C/O ratios equal to ∞, 1, 0.83, 0.68. According to Venot et al. (2015), this C/O range includes C-rich (C/O = ∞ and 1) and near-solar (C/O = 0.68) type atmospheres.

The gas mixtures and deposition times of tholins are shown in Table 1. **Although the deposition timescales differ by a factor of 100 between experiments, we have strived to obtain a film thickness leading to sufficient S/N in transmission over the VUV-MIR range. Additional effects like sputtering and electron impact from longer exposures to the plasma could further affect the properties of such films and this will be the object of further studies.** During deposition, bare silicon (10 × 10 mm) and MgF_2 windows (20 mm diameter) were placed on the bottom electrode within the PAMPRE chamber. The thickness of the deposited films is estimated from ellipsometry on the Si substrates, and the method is described in Gavilan et al. (2017). **In this paper we present the result of transmission measurements performed on the films deposited on MgF_2 windows. Synchrotron and benchtop spectrophotometers were used to measure the transmission spectra of these films in the vacuum-ultraviolet (VUV; 130 - 250 nm), the ultraviolet-visible (UV-Vis; 210 - 1000 nm), near-infrared (NIR; 1 - 3 μm) and mid-infrared (MIR; 1.43 - 10 μm) spectral ranges. These are described in more detail below.**

Although the film thickness can vary from one substrate to the other during plasma deposition, we estimate that this variation does not exceed 30% of the thickness measured on the films deposited on Si. The estimated thickness of each film is reported in Table 1. **According to Arney et al. (2017) the production of organic hazes is decreased when CO_2:CH_4 > 10. In our study, the aerosol production rate is drastically quenched at a CO_2:CH_4 ratio of 4.**

Table 1. Synthesis parameters for tholins prepared at increasing CO_2/CH_4 ratios, thickness, and Tauc gap energies.

Gas mixture N_2:CO_2:CH_4	CO_2/CH_4	Deposit [s]	Thickness [nm]	E_g [eV]
95:0:5	0	3	36 ± 7	2.35 ± 0.20
95:2.5:2.5	1	15	79 ± 16	2.54 ± 0.40
90:5:5	1	20	79 ± 16	2.49 ± 0.40
95:3:2	1.5	30	195 ± 15	3.06 ± 0.40
90:6:4	1.5	60	74 ± 40	2.66 ± 0.40
95:4:1	4	600	43 ± 21	3.20 ± 0.20
90:8:2	4	480	33 ± 16	3.23 ± 0.20

VUV transmission spectra were measured on the AU-UV beam line at the ASTRID2[2] synchrotron at Aarhus University, Denmark (Palmer et al. 2015). Thin films deposited on MgF_2 windows were placed in the *lollipop* sample holder, able to mount up to four samples. **UV-Vis transmission spectra** were measured with a bench-top UV-Vis spectrometer (*Thermo Scientific Evolution 300*). The overlapping spectral range was used to combine the VUV and UV-Vis datasets. One sample, the fully-reduced tholin, had previously been measured in the APEX[3] chamber of the DISCO[4] beam line of the SOLEIL[5] synchrotron. We confirmed that VUV spectra are reproducible between beam lines at both facilities.

Near-infrared transmission spectra were measured at the Planetary Emissivity Laboratory (DLR) using a vacuum Fourier transform infrared (FTIR) spectrometer (Bruker Vertex 80V) with a liquid nitrogen cooled HgCdTe (mercury cadmium telluride, MCT) detector at 1 cm^{-1} spectral resolution. **A Bruker A480 parallel beam accessory was mounted in front of the sample holder within the Vertex 80V to reduce artefacts due to beam reflections on the sample. This accessory helps collimate the beam when measuring highly refractive/reflective samples in transmission mode.**

Mid-infrared transmission spectra were measured with a vacuum FTIR spectrometer (Bruker Vertex 80V) available at ASTRID2. The reduced tholin mid-infrared spectrum was measured on the iN10 infrared microscope available at SOLEIL. **These were recorded at 4 cm^{-1} spectral resolution and** were corrected with a polynomial baseline to subtract the continuum absorption.

3. VUV AND MIR SPECTROSCOPY

Our spectroscopic analysis involves deconvolution of the main electronic bands for the VUV-UV spectra and of the main vibrational modes in the MIR spectra. This is done via the Levenberg-Marquardt non-linear least-squares minimization method using the IDL MPFIT routine (Markwardt 2009). **We have chosen Gaussian band shapes, suitable for characterizing molecular transitions in solids.** In fitting each band the peak position and intensity are left as free parameters, while the width is varied up to 10% between

[2] ASTRID: Aarhus STorage RIng in Demmark
[3] APEX: Atmospheric Pressure Experiment
[4] DISCO: Dichroism, Imaging and SpectrosCOpy
[5] Source Optimisée de Lumière d'Énergie Intermédiaire du LURE

spectra. Band positions and widths may shift depending on the bonding environment for each sample.

3.1. *VUV-Visible spectroscopy*

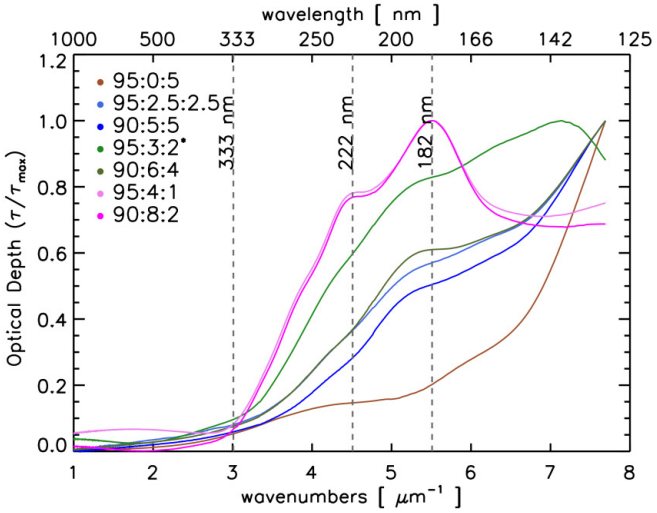

Figure 1. Vis-VUV spectra of tholins (normalized to the maximum optical depth in this range), prepared in plasmas of increasing CO_2/CH_4 ratios. Due to the large thickness (d ∼195 nm), the VUV spectrum of the 95:3:2 tholin (green curve) is saturated for wavenumbers larger than 6 μm^{-1}.

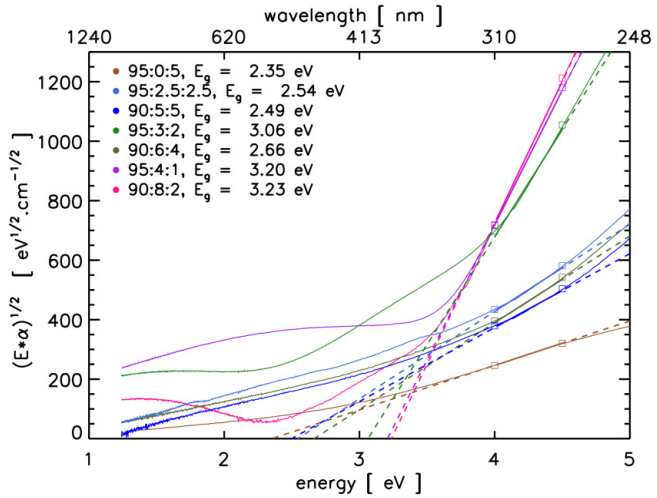

Figure 2. Tauc optical gap determination from the visible to near ultraviolet spectra for tholins prepared in plasmas with increasing CO_2/CH_4 ratios in N_2:CO_2:CH_4 mixtures.

The VUV-visible spectra of the oxidized tholins have been normalized to the maximum optical depth in the VUV. These are shown in Fig. 1. We notice that increasing the CO_2/CH_4 ratio has a direct effect on the electronic absorption bands of these tholins. This evolution is best represented by the appearance of a narrow but intense peak at ∼180 nm and a decrease in the intensity of the far-UV (FUV) band. **Varying the N_2 partial pressure from 90 to 95% has a negligible effect on the VUV spectra of tholins prepared with similar CO_2/CH_4 ratios.**

Table 2. VUV electronic bands assignments

Label	Peak pos. nm / eV	Literature position (eV)	Electronic transition	Functional group
G1	215 / 5.77	5.70[a], 5.77[b]	$n_N \rightarrow 3sa$	Amine
G2	166 / 7.47	7.14[c], 7.93[d]	$n_N \rightarrow 3pa$	Amine
G3	118 / 10.51	**10.16**[e] - 12[f]	σ - σ^*, n - σ^*	**Methyl**
G4	300 / 4.13	3.50[g] - 4.75[h]	π - π^*, n - π^*	**Carbonyl**
G5	185 / 6.7	6.2 - 7.5[i]	$n_O \rightarrow \sigma^*$	Hydroxyl
G6	241 / 5.15	5.80[j]	$n_O \rightarrow \pi^*_{CO}$	Carboxyl

[a]Hubin-Franskin et al. (2002)
[b]Tannenbaum et al. (1953)
[c]Tannenbaum et al. (1953)
[d]Harshbarger (1971)
[e]Workman (2016)
[f]Gavilan et al. (2016)
[g]Hornback (2005)
[h]Gadallah et al. (2011); Robertson & O'Reilly (1987)
[i]Xu et al. (1999)
[j]Barnes & Simpson (1963); Ari & Gven (2000)

We used the visible-near UV spectral range (250 - 1000 nm) to determine the optical band gap of these materials, **also known as the Tauc gap (Tauc et al. 1966). The gap values were obtained** by extrapolating a regression from the linear region in a $(\alpha \times E)^{1/2}$ versus E plot, where α is the absorption coefficient and E is in eV. The Tauc extrapolation is found using the linear region between the visible and near ultraviolet range, i.e. 3.8 - 4.5 eV. This region avoids the exponential absorption tail appearing in the visible energy range (1.2 - 3.8 eV), characteristic of disorder in amorphous materials, known as the Urbach tail (Jones 2012; Urbach 1953). We varied the endpoints of this range to determine the average systematic error in the gap determination. The gap values are listed in Table 1. We note that, as the CO_2/CH_4 ratio increases, so does the gap value, i.e. E_g increases from 2.35 to 3.20 eV. **These gap values are consistent (within the error bar) with those found via the ellipsometry on similar films deposited on Si substrates (Gavilan et al. 2017), validating the coherence of both methods.**

As seen in Fig. 1, the VUV-visible spectral profile for samples prepared with the same CO_2/CH_4 ratio are similar, e.g. 95:4:1 and 90:8:2 both with a ratio of 4 and 95:2.5:2.5 and 90:5:5 both with a ratio of 1. Because

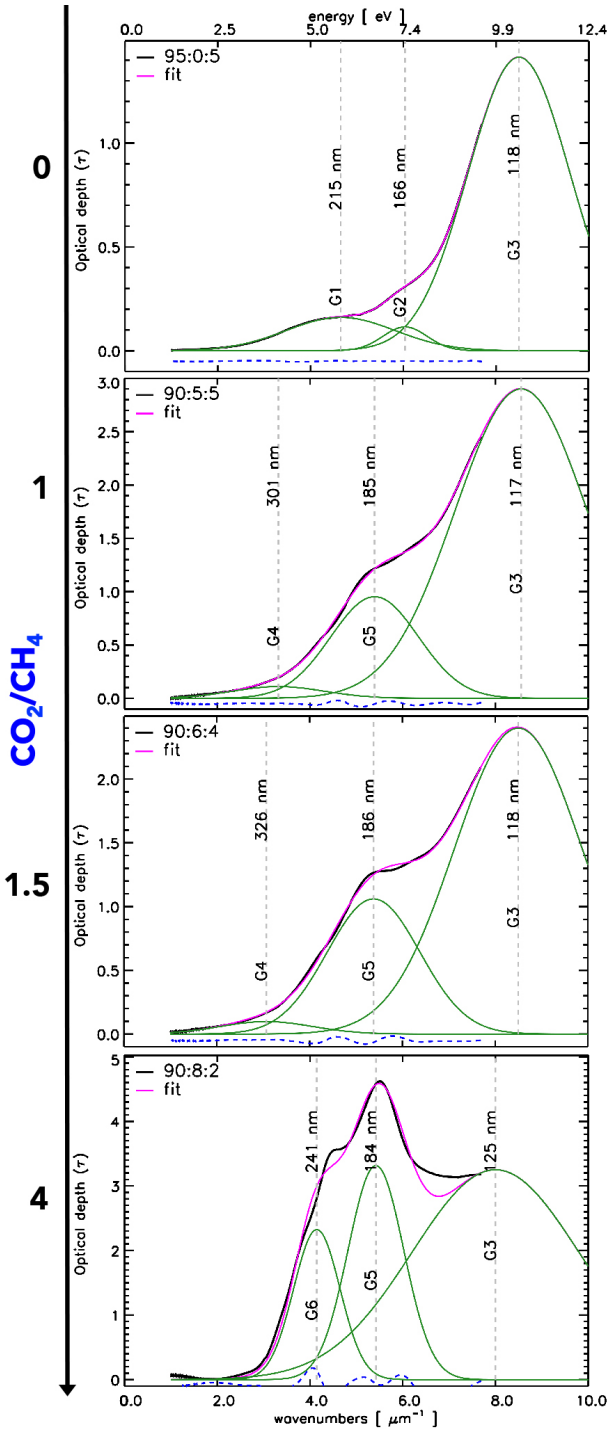

Figure 3. Spectral deconvolution of the Vis-VUV of increasingly oxidized organic tholins prepared in plasmas of increasing CO_2/CH_4 ratios.

the spectra of the 95:3:2 sample is optically saturated in the VUV, we chose the 90 % N_2 series to deconvolve the VUV-vis spectra for increasing CO_2/CH_4 ratios = 0, 1, 1.5, 4. The resulting deconvolution is shown in Fig. 3.

VUV-visible spectra reveal transitions of electrons between the molecular orbitals of organic materials. **Identification of possible carriers of the electronic bands in our tholins is done by comparison to UV-Vis gas phase spectra of common chromophores present in organic molecules (e.g. Hornback 2005; Workman 2016). These are listed in Table 2. The major electronic transitions in organic compounds are $\sigma \rightarrow \sigma^*$, $\pi \rightarrow \pi^*$, $n \rightarrow \sigma^*$ and $n \rightarrow \pi^*$, and associated bands.** Generally π-electronic transitions are found at **$1.6 < \lambda^{-1} < 5$ μm^{-1} ($200 < \lambda < 600$ nm), while σ-electronic transitions are found at higher energies, $\lambda^{-1} > 3.8$ μm^{-1} ($\lambda < 260$ nm)** (Gadallah et al. 2011; Gavilan et al. 2016).

For our sample spectra each VUV-Vis spectrum can be deconvolved into three main bands. However, as the oxidation degree increases, band and peak positions are modified. For the tholin with no CO_2, two bands, which we call G1 and G2 are attributed to transitions in amine functional groups. G1 and G2 are assigned to electronic transitions from the lone-pair electrons on nitrogen to nitrogen atomic-like orbitals (Hubin-Franskin et al. 2002; Duarte et al. 2013). The largest band, called G3, found in the far-UV, is generally attributed to σ - σ^* and n - σ^* type transitions and its peak position is found at **$8 < \lambda^{-1} < 8.5$ μm^{-1} (118 - 125 nm)**.

The VUV spectra evolve as the oxidation degree increases. The spectra for samples with $CO_2/CH_4 = 1$ and 1.5 are remarkably similar. The smaller UV bands have shifted, which signals the molecular evolution of the solid. G4 is then attributed to low energy π - π^* and n - π^* transitions arising from structural disorder (Gadallah et al. 2011). G5 is a new VUV band centered at λ^{-1} **$\sim$5.4 μm^{-1} (185 nm)**, whose intensity increases with increasing oxidation degree, and is attributed to electronic transitions in hydroxyl groups due to the promotion of an electron from the highest filled molecular orbital to an antibonding orbital (σ^*_{OH}) (Duarte et al. 2013). This band usually appears at **$5 < \lambda^{-1} < 6.1$ μm^{-1} (165 - 200 nm)** (Xu et al. 1999).

Finally, for the most oxidized sample, with $CO_2/CH_4 = 4$, the G5 band is most prominent as a consequence of the larger number of oxygenated bonds. G6 is a new band appearing at λ^{-1} **$\sim$4.2 μm^{-1} (240 nm)** and is assigned to the $n_O \rightarrow \pi^*_{CO}$ transitions from the lone-pair orbital on the carbonyl oxygen to the antibonding π_{CO} valence orbital (Barnes & Simpson 1963; Ari & Gven 2000) or to the valence shell excitations of hydroxyl groups (Duarte et al. 2013). For this sample the position of G3 is shifted to lower energies and its relative intensity decreases, indicating a loss of σ-bonds.

3.2. *Mid-infrared spectroscopy*

The mid-infrared spectra of our samples were split into three spectral ranges corresponding to the most intense **vibrational** bands in the mid-infrared: **a) amines (3800 - 2400 cm^{-1}), b) nitriles (2300 - 2050 cm^{-1}), and a c) hetero-aromatics band (1900 - 1000 cm^{-1})** (Mutsukura 1999; Imanaka et al. 2004). We have deconvolved the main mid-infrared spectral bands of all samples prepared with a 95 % N_2 concentration, corresponding to the following N_2:CO_2:CH_4 mixtures: 95:0:5, 95:2.5:2.5, 95:3:2, and 95:4:1, plotted in Fig. 4. Such deconvolution provides further insight into the evolution of the molecular structure of organic aerosols as a function of their oxidation degree. **In this first order analysis, we use Gaussian functions to fit the most intense vibrational modes due to broad bonding distributions in the solid network that result in statistical bell curves, and neglect any perturbations to the line shape due to secondary resonances. Fitting vibrational bands is done by considering the maximum number of Gaussians needed to characterize the vibrational spectra of the CO_2/CH_4 = 0 tholin, which has the largest number of peaks. To fit the tholin spectra at different oxidation degrees we have assumed that: 1) the organic network of tholins may be similar to first order, 2) oxidation will produce new bonds that may shift the energies and abundances of functional groups.**

For tholins prepared with increasing CO_2/CH_4 ratios, two main features appear in the amine band. These are attributed to the stretching modes of NH functions in amide groups at ∼3180 cm^{-1} and to aldehyde CH stretching modes at ∼2800 cm^{-1}. In the nitrile band increasing oxidation translates into a decrease of singly-bonded and aromatic isonitriles at ∼2140 cm^{-1} and ∼2105 cm^{-1} respectively and to the decrease of singly-bonded nitrile modes at ∼2240 cm^{-1}. **In contrast at CO_2/CH_4 ratios greater than 1 we note the effect of increasing oxidation on the heteroaromatic band: the unsaturated C=C and C=N modes decrease while the intensity of the carbonyl (C=O) band at 1700 cm^{-1}, increases. This is confirmed by the formation of a new band in the region between 1550 and 1300 cm^{-1}, attributed to bending modes in NH_2, $CH_{2,3}$, and C-OH functional groups**.

From the deconvolution of the amines band an increasing CO_2/CH_4 ratio results in the rapid evolution of the NH stretching mode associated with amides and to the aldehyde CH stretch. Although the primary NH bonds associated with amines are present and common for all samples, in samples with a CO_2/CH_4 = 4 ratio the NH band associated with amides is relatively more intense. At maximum oxidation there is also a loss of the aliphatic CH stretching band, suggesting a decreased C/N ratio in the most oxidized materials. The deconvolution of the nitrile band shows the progressive loss of isonitrile modes with increasing oxidation. Together with the loss of singly-bonded nitriles, this suggests a gain in disorder in the structure of oxidized tholins. Mass loss through nitriles with respect to the amine and hetero-aromatic bands is a significant effect of oxidation.

Due to the large number of overlapping stretching and bending modes deconvolution of the hetero-aromatic band is performed by simplifying the number of participant modes. The region between 1500 - 1300 cm^{-1} is attributed to a large peak including the overlapping contribution of bending modes from CH, NH and OH groups. As the CO_2/CH_4 ratio increases the C=O stretching mode at ∼1700 cm^{-1} increases, while the relative intensities of the C=N and aromatic C=C stretching modes decrease. In the plasma oxidation is due to O atoms

Table 3. Mid-infrared band assignments for tholins prepared at increasing CO_2/CH_4 ratios.

Peak (cm^{-1})	Range (cm^{-1})	Band assignments[a,b]
3320	3500-3100	NH/NH_2 stretch (Amine I)
3200		NH stretch (Amine I)
3175		NH stretch (Amide I)
2960	3000-2800	CH stretch (ali. CH_2/CH_3, arom. =CH)
2846	2900-2800	aldehyde CH stretch (H-(R)C=O)
2240	2260-2230	R-C≡N, nitrile stretch
2180	2230-2150	C=C-CN conjugated nitrile stretch[c]
2145	2180-2120	R-N≡C, isonitrile stretch[d]
2110	2120-2100	aromatic -N≡C stretch
1700	1730-1680	C=O stretch
		Also: carbonyl (aldehyde, ketone), carboxyl
1625	1650-1620	C=N stretch
		Also: C=O, C=C stretch
1560	1570-1540	C=C stretch
		Also: C=N, quinones, carboxylates, NO
1460	1480-1440	**$CH_{2,3}$, NH_2, C-OH bending**
1350	1370-1340	$CH_{2,3}$ bending
		Also: aromatic C-N bending, N-O stretch
1230	1250-1220	C-O stretch
		Also: C-OH stretch, ester

[a] http://webbook.nist.gov/chemistry/
[b] https://webspectra.chem.ucla.edu/irtable.html
[c] Imanaka et al. (2004)
[d] Mutsukura (1999)

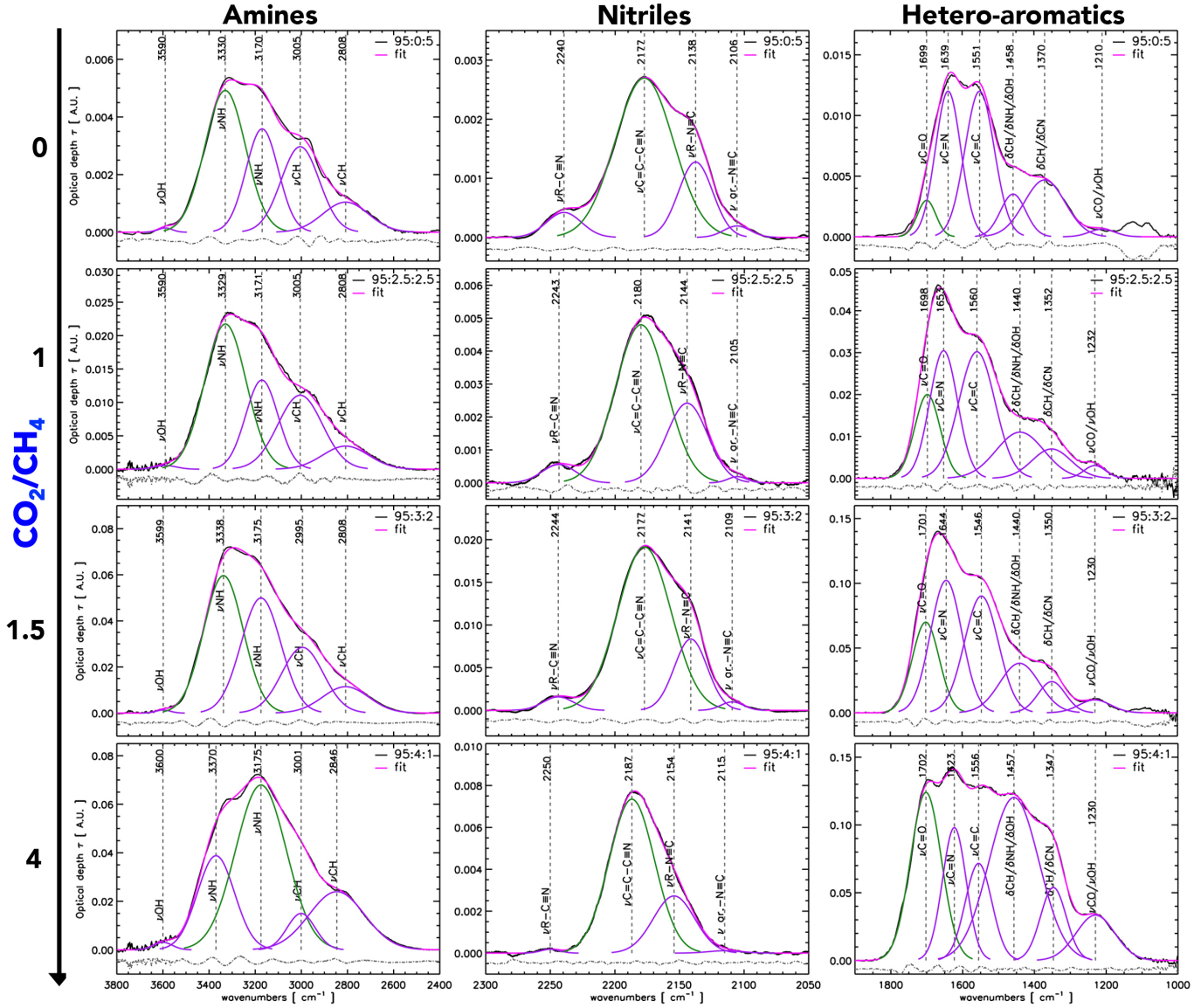

Figure 4. Spectral deconvolution of the main mid-infrared spectral bands (amines, nitriles, hetero-aromatics spanning 3800-1000 cm^{-1}) of increasingly oxidized organic tholins. To illustrate the effect of the increasing CO_2/CH_4 ratio on the molecular structure, only tholins from the same series (95 % N_2) and varying CO_2/CH_4 ratios = 0, 1, 1.5 and 4, are used.

and OH radicals produced in the dissociation of CO_2 and CH_4 molecules. As the oxidation degree increases, the formation of NH and C-N bonds are favored relative to C=N bonds. We also note that, even without CO_2 in the gas mixture, the C=O mode is present in the reduced tholin. **This could be due to surface oxidation by O_2 in air whilst transporting the sample for analysis or to trace oxygen species present in the plasma**.

3.3. *Absolute imaginary indices*

Transmission spectra in the VUV-visible, near-infrared and mid-infrared ranges for each sample and the thicknesses listed in Table 1 are used to **estimate the wavelength-dependent imaginary index k(ν), over this spectral region, by means of the relation,**

$$k(\nu) = \frac{\tau(\nu)}{4\pi\nu d}, \tag{2}$$

where $\tau(\nu)$ is the optical depth, ν is the frequency, and d is the sample thickness. The result is shown in Fig. 5. The progressive increase of oxidation in these organic materials directly results in the increase of the absolute absorption over the entire wavelength range (from 0.13 to 9 μm). For the most oxidized tholin, C/O = 0.68, the absolute absorption

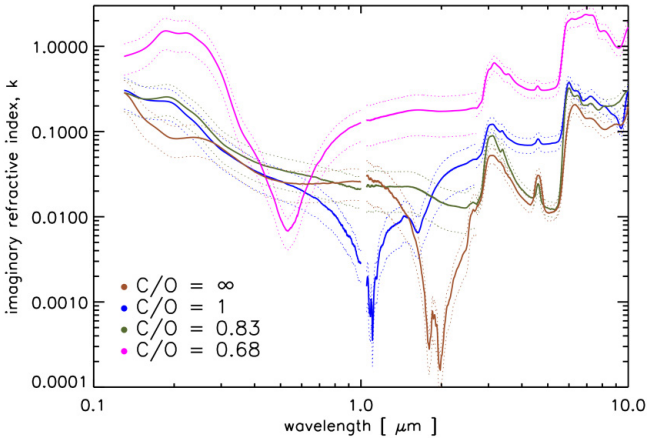

Figure 5. Imaginary refractive index k spanning the VUV-Vis, NIR and MIR ranges for tholins prepared at increasing CO_2/CH_4 or C/O ratios. As oxidation increases the absorption coefficient increases steeply in the ultraviolet range (130 - 300 nm), linearly in the mid-infrared, while the k inversion region is blueshifted.

increases most prominently in the the VUV, 0.13 - 0.2 μm, and UV, 0.2 - 0.3 μm, in agreement with previous results reported in Gavilan et al. (2017).

In the mid-infrared the most absorptive region corresponds to the hetero-aromatic band, which increases linearly with C/O ratio. We also note a significant drop of k over two orders of magnitude from the VUV to the visible region (0.13 - 1 μm) for the most reduced sample, the Titan type tholin with C/O = ∞. McKay et al. (2001) showed this drop is essential for reproducing the shape of Titan's geometric albedo.

The uncertainty in near-infrared absorption is larger due to the lower absorption indices in this region, where k $\leq$ 0.2. The absorption in the near-infrared increases with oxidation due to the presence of second and third overtones of NH, NH_2 and OH vibrations. This region is also characterized by absorption minima. An inversion of k is present at 1.8 - 2 μm for the C/O = ∞ tholin, and the position of this inversion feature blueshifts towards 0.9 - 1.1 μm for the tholin with C/O = 1 and to 0.5 - 0.6 μm for the tholin with C/O = 4. However, this k inversion is absent from the tholin corresponding to C/O = 0.83 (90:6:4). Although this sample is more oxidized, as seen by the decrease in nitrile intensity and the oxidation of the amine and hetero-aromatic bands, the lack of a minimum imaginary absorption index is surprising. This may be explained by the peculiar plasma conditions produced at a ratio of $CO_2/CH_4 = 1.5$. At this ratio the plasma attains a peculiar (dis-)equilibrium where tholin production is enhanced rather than quenched. Further experiments with this particular gas mixture should unveil the gas kinetics of this plasma and its effects on aerosol production.

4. VUV IRRADIATION OF THOLINS

Two tholins prepared with a ratio of $CO_2/CH_4 = 1$ were irradiated with a monochromatic beam of 160 nm photons. The VUV-visible spectra of the samples were measured before, τ_o, and after irradiation, τ_{irr}.

In all cases, a slight decrease in the spectral intensity in the 5.5 - 7 μm^{-1} (200 - 150 nm) region is attributed to the VUV photolysis of aromatic C=O structures. In contrast, we note the intensity growth of the 3.5 - 4.5 μm^{-1} (200 - 300 nm) region, attributed to π-bond formation of the organic matrix. The photon flux the beam line produces was measured using an AXUV100G photodiode. Using the known responsivity of this diode, at λ = 160 nm there are 6.7 $\times$ 10^{11} photons/sec/100 mA. During the irradiation the beam current was recorded every second and the total fluence was calculated based on the average beam current ($\sim$180 mA). The 90:5:5 sample received a dose of $\sim$5 $\times$ 10^{17} eV cm^{-2} while the 90:6:4 sample received a dose of $\sim$8 $\times$ 10^{17} eV cm^{-2}.

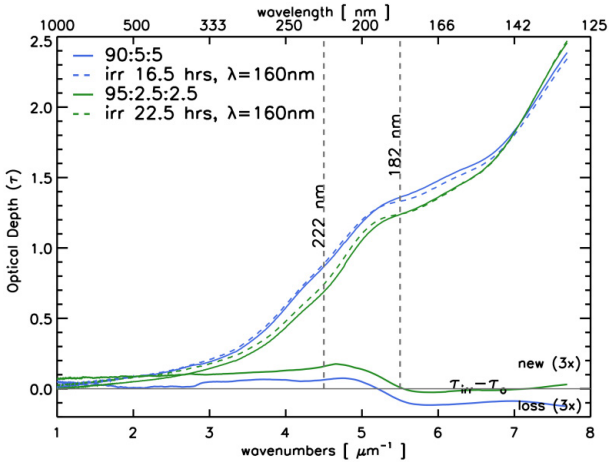

Figure 6. Vis-VUV spectra of oxidized tholins irradiated with VUV photons. The τ_{irr}-τ_o lines around 0 show the new and lost band intensities **(scaled by a factor of 3)**.

These results are consistent with previous VUV irradiation experiments performed by Gadallah et al. (2011) on hydrogenated amorphous carbon (HAC) materials. They used a deuterium lamp, whose emission peaks at 160 nm, and irradiated carbonaceous thin films with doses of at least 10^{22} eV cm^{-2}. UV spectra of the irradiated HAC samples showed an increase of the sp^2 carbon fraction, giving rise to π - π^* electronic transitions peaking at λ^{-1} $\sim$**4.6** μ**m**$^{-1}$ **(217 nm)**. Our irradiation experiments confirm that structural modifications can

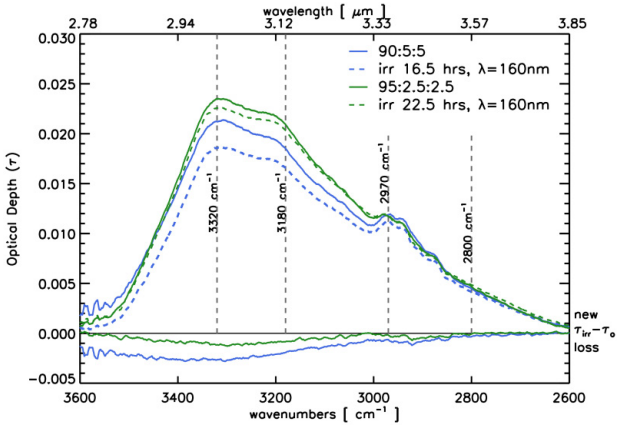

(a)

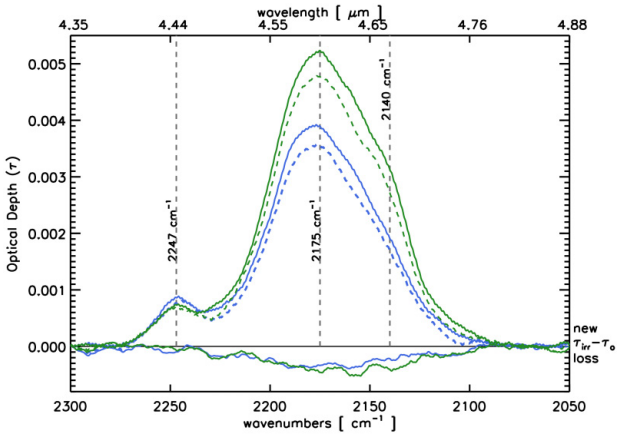

(b)

Figure 7. Mid-infrared spectra (normalized) of VUV-irradiated tholins showing the evolution of the a) amine (3600 - 2600 cm^{-1}), and b) nitrile (2300 - 2050 cm^{-1}) bands.

arise at lower UV fluences in organic materials. During irradiation, the transmission of the MgF_2 window could also evolve due to VUV photon absorption. However, as MgF_2 is a non-organic crystal, the growth of new bands in the 200 - 300 nm range is attributed to the evolution of organic tholin.

The mid-infrared spectra of the VUV irradiated samples were measured before and after irradiation. Following irradiation the amine band shows the greatest loss in intensity. This loss is most marked for amines in the 3400 - 3200 cm^{-1} region, with a maximum loss at ∼3300 cm^{-1}. The lower frequency modes in the amines region, including the CH and OH bands around 3000 - 2600 cm^{-1}, are little affected. Following VUV irradiation, the nitrile band shows a general depletion with a maximum loss of conjugated nitriles. **Both mass loss (desorption) and photolysis (inducing fragmentation and/or bond creation) could concur during the VUV irradiation of tholins. Further experiments are required to unveil which mechanism is responsible for the photo-degradation effects.**

To compare the laboratory UV doses to the radiation from an exoplanet host star, we use the UV spectra of GJ876, an M dwarf observed by the International Ultraviolet Explorer (IUE) (Linsky 2014). In this study, the spectral flux is rescaled to the distance of its habitable zone (0.21 astronomical units, AU). We consider the flux of GJ876 at λ = 160 nm, of ∼8 ergs cm^{-2} s^{-1}, corresponding to the monochromatic photons used at the synchrotron. The laboratory doses are then equivalent to exposure times of ∼28 hours (for the 90:5:5 tholin) and ∼45 hours (for the 95:2.5:2.5 tholin) at 0.21 AU of GJ876. Considering the slow formation lifetimes of oxidized organic aerosol, our laboratory spectra of photo-degraded tholins could be relevant to future observations of exoplanetary hazes.

5. DISCUSSION

Future space telescopes like ARIEL and LUVOIR will enable the investigation of exoplanets ranging from Jupiter- and Neptune-size down to super-Earth and Earth-size. ARIEL instruments are expected to cover the visible and infrared 0.5 - 7.8 μm range (Tinetti et al. 2016), while LUVOIR will enable multi-wavelength observations covering the ultraviolet to near-infrared from 0.2 - 2.5 μm.

Our spectroscopic VUV-MIR study covering the 0.13 - 10 μm range can thus provide relevant laboratory constraints for the future observations of exoplanet atmospheres. The spectra of oxidized aerosols signals a distinct large absorption in the 0.13 - 0.4 μm range and a flatter but strong absorption band in the 6 - 7.5 μm range relative to reduced aerosols. This high absorption coefficient may increase the detectability of exoplanet atmospheres where hazes form under oxidizing conditions. Together with a weaker nitrile band and a minimum absorption window in the visible range, these constitute potential observables of atmospheric oxidation. **Organic aerosols constitute potential exoplanet atmospheric biosignatures, as organic hazes can be derived from biogenic methane (Catling et al. 2017), although abiotic sources are not discarded. While the simultaneous detection of CO_2 and CH_4 in an habitable exoplanet atmosphere has been recently proposed as a potential biosignature (Krissansen-Totton et al. 2018), en-**

suing oxidized organic hazes could also constitute observable biosignatures.

6. CONCLUSIONS

We have produced laboratory analogs of oxidized organic aerosols. These were prepared in increasingly oxidizing plasmas from mixtures of N_2:CO_2:CH_4, characterized by an increasing CO_2/CH_4 ratio from 0 (fully reducing) to 4. These correspond to atmospheres with C/O ratios from 0.68, 0.83, 1 and ∞, i.e. representative of carbon-poor, solar-like to carbon-rich atmospheres. The samples were characterized via transmission spectroscopy from the vacuum-ultraviolet to the mid-infrared.

- **The molecular and electronic structure of these materials is dominated by the CO_2/CH_4 ratio in the N_2:CO_2:CH_4 gas mixture**. Ultraviolet spectroscopy revealed the presence of π - π^* and n - π^* transitions in the **2** $< \lambda^{-1} <$ **5** μ**m**$^{-1}$ **(200 - 500 nm)** range in all samples. These are attributed to electronic transitions in amine bonds for tholins prepared in fully reducing conditions. As the CO_2/CH_4 ratio increases new bands emerge in this range, attributed to electronic transitions in hydroxyl and carboxyl bonds. For all cases a large absorption band in the far ultraviolet is present and is attributed to σ - σ^* and n - σ^* electronic transitions.
- Infrared spectroscopy revealed the formation of oxygenated bonds with increasing CO_2/CH_4 ratio including stretching modes from NH, OH, C=O, C=N and the formation of a new band in the $\sim$1400 - 1300 cm^{-1} region which could be attributed to NH, C-N, OH, C-O bonds, as expected in CHON rich organic matter. The decomposition of the nitriles band revealed the loss of aromatic nitriles and singly bonded R-N=C=N modes with oxidation.
- The absolute absorption index increases linearly for all samples with increasing degrees of oxidation. The absorption is greatest in the VUV-UV range from 0.13 - 3 μm for the most oxidized samples which are also most opaque in the 6 - 10 μm hetero-aromatic band region. Oxidized aerosols show a weaker nitrile band and a blue-shifted absorption minimum compared to reduced aerosols.
- VUV irradiation of oxygenated aerosols revealed the formation of new π - π^* bands in the **4** $< \lambda^{-1} <$ **5** μ**m**$^{-1}$ **(200 - 250 nm)** region and the loss of electronic bands below 200 nm, corresponding to the formation of NH, C-N, OH bonds and the loss of amines and isonitriles observed in their MIR spectra.
- Our results suggest that oxidative plasma chemistry can result in solids with complex oxygenated bonds leading to solids that are more opaque in the VUV-MIR range. Because of their high absorption properties, oxidized organic aerosols could improve the detectability of exoplanet atmospheres. This spectral signature is indicative of the presence of oxic atmospheric conditions and could offer a potential biosignature for photosynthetic life.

Acknowledgements. We thank the staff at the ASTRID2 synchrotron for their help and access to beam time. We thank A. Giuliani for the preliminary VUV measurement of the reduced tholin sample at the DISCO beam line of the SOLEIL synchrotron (project No. 20160171) and E. Dartois for kindly supplying the DISCO-adapted sample holder. We thank A. Maturilli for his help with the near infrared measurements at the Planetary Emissivity Laboratory (DLR). L.G. recognizes support for this visit from the Europlanet Research Infrastructure funded by the European Union's Horizon 2020 research and innovation programme under grant agreement No 654208. NJM recognizes support from the COST Action TD1308 *Origins*. N.C. and L.G. thank the European Research Council for funding via the ERC *PrimChem* project (grant agreement No. 636829.)

Software: MPFIT, (Markwardt 2009)

REFERENCES

Ari, T., & Gven, M. H. 2000, Journal of Electron Spectroscopy and Related Phenomena, 106, 29

Arney, G. N., Meadows, V. S., Domagal-Goldman, S. D., et al. 2017, ApJ, 836, 49

Barnes, E. E., & Simpson, W. T. 1963, JChPh, 39, 670

Catling, D. C., Krissansen-Totton, J., Kiang, N. Y., et al. 2017, ArXiv e-prints, arXiv:1705.06381

Duarte, A. A., Gomes, P. J., Ribeiro, J. H. F., et al. 2013, The European Physical Journal E, 36, 98

Feulner, G. 2012, Reviews of Geophysics, 50, RG2006

Fleury, B., Carrasco, N., Millan, M., Vettier, L., & Szopa, C. 2017, Earth and Planetary Science Letters, 479, 34

Gadallah, K. A. K., Mutschke, H., & Jäger, C. 2011, A&A, 528, A56

Gavilan, L., Alata, I., Le, K. C., et al. 2016, A&A, 586, A106

Gavilan, L., Broch, L., Carrasco, N., Fleury, B., & Vettier, L. 2017, ApJL, 848, L5

Haqq-Misra, J. D., Domagal-Goldman, S. D., Kasting, P. J., & Kasting, J. F. 2008, Astrobiology, 8, 1127

Harshbarger, W. R. 1971, JChPh, 54, 2504

Hornback, J. 2005, Organic Chemistry (Cengage Learning)

Hubin-Franskin, M.-J., Delwiche, J., Giuliani, A., et al. 2002, JChPh, 116, 9261

Imanaka, H., Khare, B. N., Elsila, J. E., et al. 2004, Icarus, 168, 344

Jacobson, M. C., Hansson, H. C., Noone, K. J., & Charlson, R. J. 2000, Reviews of Geophysics, 38, 267

Jones, A. P. 2012, A&A, 540, A2

Kasting, J. F. 1993, Science, 259, 920

Krissansen-Totton, J., Olson, S., & Catling, D. C. 2018, Science Advances, 4, eaao5747

Lavvas, P., & Koskinen, T. 2017, ArXiv e-prints, arXiv:1708.09257

Lavvas, P., Yelle, R. V., Koskinen, T., et al. 2013, Proceedings of the National Academy of Sciences, 110, 2729

Linsky, J. 2014, Challenges, 5, 351

Madhusudhan, N., Agúndez, M., Moses, J. I., & Hu, Y. 2016, SSRv, 205, 285

Mahjoub, A., Carrasco, N., Dahoo, P.-R., et al. 2012, Icarus, 221, 670

Markwardt, C. B. 2009, Proc. Astronomical Data Analysis Software and Systems XVIII, 411, 251

Marley, M. S., Ackerman, A. S., Cuzzi, J. N., & Kitzmann, D. 2013, Clouds and Hazes in Exoplanet Atmospheres (Mackwell, S. J. and Simon-Miller, A. A. and Harder, J. W. and Bullock, M. A.), 367–391

McKay, C. P., Coustenis, A., Samuelson, R. E., et al. 2001, Planet. Space Sci., 49, 79

Mutsukura, N. 1999, Thin Solid Films, 349, 115

Palmer, M. H., Ridley, T., Hoffmann, S. V., et al. 2015, JChPh, 142, 134302

Pavlov, A. A., Brown, L. L., & Kasting, J. F. 2001, J. Geophys. Res., 106, 23267

Robertson, J., & O'Reilly, E. P. 1987, PhRvB, 35, 2946

Sciamma-O'Brien, E., Dahoo, P.-R., Hadamcik, E., et al. 2012, Icarus, 218, 356

Swain, M. R., Vasisht, G., & Tinetti, G. 2008, Nature, 452, 329

Swain, M. R., Vasisht, G., Tinetti, G., et al. 2009a, ApJL, 690, L114

Swain, M. R., Tinetti, G., Vasisht, G., et al. 2009b, ApJ, 704, 1616

Szopa, C., Cernogora, G., Boufendi, L., Correia, J. J., & Coll, P. 2006, Planetary and Space Science, 54, 394

Tannenbaum, E., Coffin, E. M., & Harrison, A. J. 1953, JChPh, 21, 311

Tauc, J., Grigorovici, R., & Vancu, A. 1966, Physica Status Solidi B-basic Solid State Physics, 15, 627

Tinetti, G., Drossart, P., Eccleston, P., et al. 2016, in Proc. SPIE, Vol. 9904, Space Telescopes and Instrumentation 2016: Optical, Infrared, and Millimeter Wave, 99041X

Trainer, M. G., Pavlov, A. A., Dewitt, H. L., et al. 2006, Proceedings of the National Academy of Science, 103, 18035

Urbach, F. 1953, Physical Review, 92, 1324

Venot, O., Hébrard, E., Agúndez, M., Decin, L., & Bounaceur, R. 2015, A&A, 577, A33

Venot, O., Bénilan, Y., Fray, N., et al. 2017, ArXiv e-prints, arXiv:1709.08415

von Paris, P., Rauer, H., Lee Grenfell, J., et al. 2008, Planetary and Space Science, 56, 1244

Wilson, E. H., & Atreya, S. K. 2004, Journal of Geophysical Research (Planets), 109, E06002

Wolf, E. T., & Toon, O. B. 2010, Science, 328, 1266

Workman, J. 2016, Concise Handbook Of Analytical Spectroscopy, The: Theory, Applications, And Reference Materials (In 5 Volumes) (World Scientific Publishing Company)

Xu, K., Amaral, G., & Zhang, J. 1999, JChPh, 111, 6271